E.K. Anderson, T.D. Aslam, S.I. Jackson.
"Analysis of Adjacent Detonating Explosive Slabs."
In Proceedings of the 15th International Detonation Symposium, Office of Naval Research, pp. 693-702 (Office of Naval Research, 2015)

Analysis of Adjacent Detonating Explosive Slabs

Eric K. Anderson, Tariq D. Aslam, Scott I. Jackson
Shock and Detonation Physics Group
Weapons Experiments Division
Los Alamos National Laboratory
Los Alamos, New Mexico, USA

Abstract. A test series was conducted to investigate explosive assemblies consisting of a rectangular PBX 9501 slab bonded on one side to a PBX 9502 slab. PBX 9501 layers of sufficient thickness drove a transverse shock in the PBX 9502 with an eventual transition to detonation. Here, we describe an analytic modeling strategy that couples the Detonation Shock Dynamics (DSD) model to compute the PBX 9501 front shape and phase velocity with shock-polar analysis to model the interaction between the explosive slabs. The effect of DSD boundary conditions on the results are investigated, and we also compare results of the model to experiments.

Introduction

Recent tests showed that in explosive assemblies, each consisting of a PBX 9502 slab bonded on one side to a PBX 9501 slab, faster detonation in the PBX 9501 could transversely initiate detonation in the PBX 9502 [1,2]. A simplified diagram is provided in Fig. 1, where the shock structure is shown at three different points in time. The PBX 9501 detonation drives an oblique shock in the PBX 9502, which transitions to detonation some distance from the interface between the two explosives. We refer to the region of the PBX 9502 slab between the interface of the two explosives and the transition to detonation as initiating layer. In the experimental tests, the pressure associated with the PBX 9501 detonation was varied by changing the thickness of the PBX 9501 slab. Increasing the PBX 9501 slab thickness resulted in reduced initiating layer thickness, and the pressure vs. time-to-detonation relationship was in good agreement with one-dimensional (1D) shock-to-detonation transition (SDT) experiments [3].

While previous results suggest that it may be possible to predict initiating layer thickness given a known shock pressure in the PBX 9501 [3], no simple models exist to predict the steady behavior of both explosives in the two-layer assemblies. However, similar behavior has been observed by Matignon et al. [4] in an analogous cylindrical arrangement, where a cylinder of one explosive was surrounded by a tube of a faster explosive. They modeled the interaction between the two explosives using shock polar analysis, and were able to compute shock angles in the driven explosive with reasonable accuracy.

In the present work, we explore the possibility of combining DSD with polar analysis to predict the behavior of the bonded slab assemblies. The pro-

Approved for unlimited release: LA-UR-14-24816

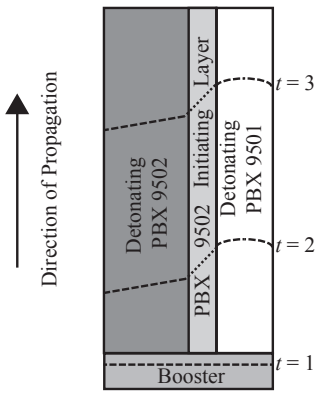

Fig. 1. Given sufficient PBX 9501 layer thickness, the steady structure shown at time $t = 2$ and $t = 3$ develops, where a PBX 9501 detonation causes the generation of an initiating layer in the PBX 9502. A transition to detonation occurs in the PBX 9502 further from the interface.

posed method involves using DSD to predict the detonation front shape and phase velocity in the PBX 9501. The DSD-generated front-shape would then be used to extract a representative shock angle in the PBX 9501 detonation. The PBX 9501 detonation near the interface between the explosives would then be modeled as a planar, oblique detonation with this representative shock angle. This simplification would allow the use of polar analysis to predict the shock angle and associated pressure of the PBX 9502 initiating layer shock. Given this pressure, we have shown in previous work that the PBX 9502 initiating layer thickness[3] can be predicted. We apply this method to three experimental cases in the present work, and compare computed results with those observed experimentally.

PBX 9501 Front Shape Results and DSD Predictions

For each of the assemblies listed in Table 1, a streak camera image of the detonation breakout was combined with a phase velocity measurement to obtain a profile of the detonation front. This process is described in detail elsewhere[1], but the results for the assemblies with 1.55, 2.00, and 2.5 mm PBX 9501 layers are shown in Figs. 2–4, by symbols representing points measured on the streak camera image. In the figures, only the PBX 9501 portion of the detonation fronts are shown, and the interface with the PBX 9502 is on the left.

Table 1. Measured densities and phase velocities (D_0) for experimental tests.

PBX 9501 Thickness (mm)	PBX 9501 Density (g/cm^3)	PBX 9502 Density (g/cm^3)	D_0 $\left(\frac{\text{mm}}{\mu\text{s}}\right)$
1.55	1.8355	1.8722	8.638
2.00	1.8327	1.8704	8.696
2.5	1.8342	1.8675	8.731

Fitting Experimental Front Shape Data

For the dual slab assemblies under consideration, the PBX 9501 slab is subject to different boundary conditions on each side. This results in an asymmetric front shape, requiring modification of the fitting form commonly used for symmetric fronts. For this reason, the following piecewise functional form, based on the established fitting form described by Jackson and Short[5], was used:

$$z(x) = \begin{cases} A_1 \ln\left[\cos\left[\eta_1 \frac{\pi}{2} \frac{x-B_1}{X}\right]\right] + C_1 + S : x < S \\ A_2 \ln\left[\cos\left[\eta_2 \frac{\pi}{2} \frac{x-B_2}{X}\right]\right] + C_2 + S : x \geqslant S. \end{cases}$$

In this function, z represents distance in the direction of detonation propagation, and x is the distance from the center of the slab. The term X represents the half-thickness of the slab, while parameters A_1, A_2, η_1, and η_2 are allowed to vary to achieve a fit. Parameters B_1 and B_2 allow for the function maximum to shift away from $x = 0$, C_1 and C_2 allow for a shift in the vertical (z) direction, and S is the x coordinate where the piecewise function splits to accommodate the different boundary conditions on each side of the PBX 9501 slab.

The constraints imposed on the fitting algorithm are to require continuity at $x = S$ in the function as well as its first and second derivatives. In addition, S is required to be the maximum of both sides of the piecewise function, which is imposed by requiring $B_1 = B_2 = S$. Subject to these constraints, the

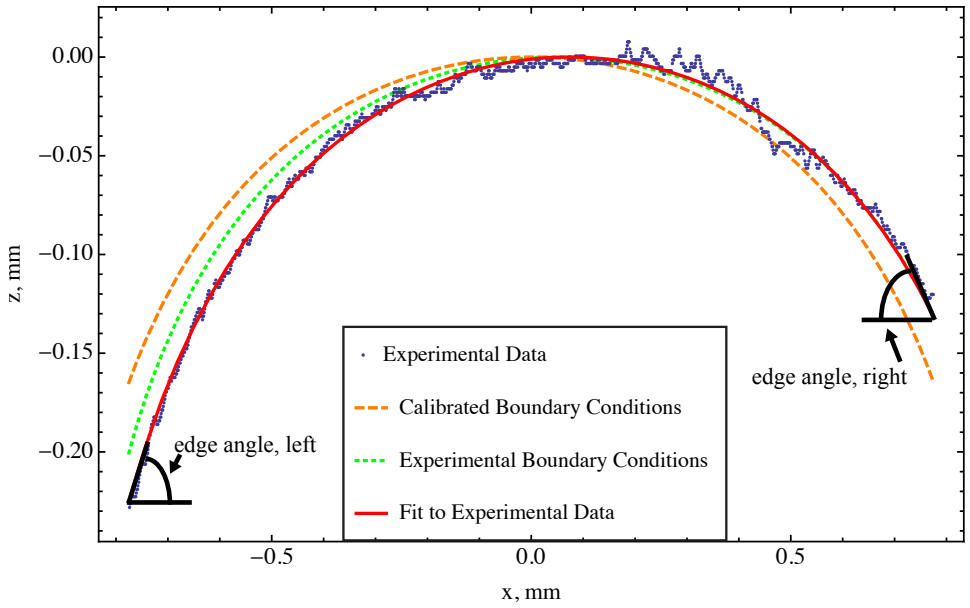

Fig. 2. Front curvature data and fits for the case of the 1.55 mm PBX 9501 layer. The edge angles of Table 2 are shown graphically.

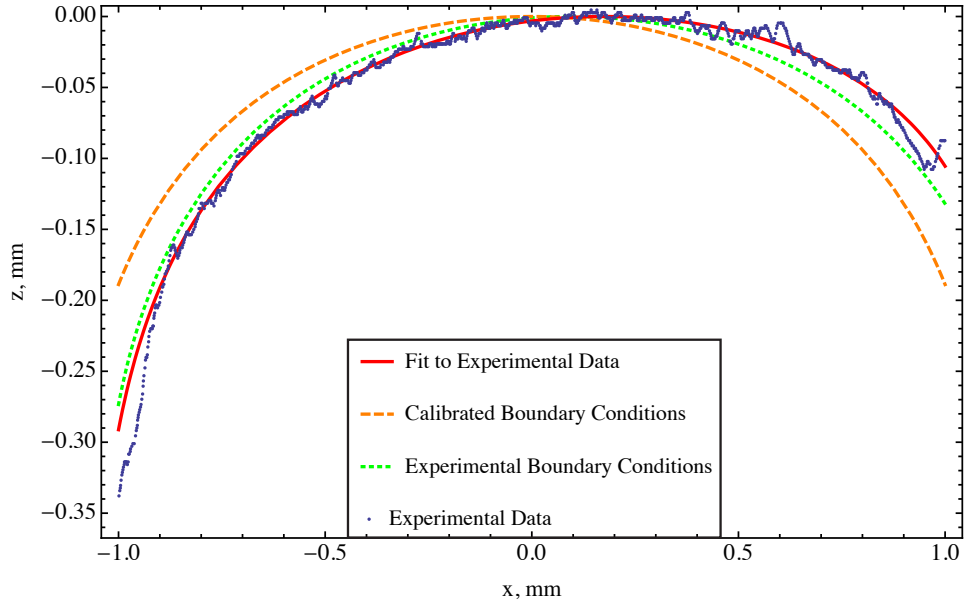

Fig. 3. Front curvature data and fits for the case of the 2.00 mm PBX 9501 layer.

parameters are determined by minimizing the sum of the squares of the fit residuals.

The resulting fits are shown for each experiment by the solid line in Figs. 2-4. The quality of each fit is characterized in Table 2 as the norm of the difference between each experimental data point and the function value corresponding to that x-location on the detonation front. In addition, Table 2 shows

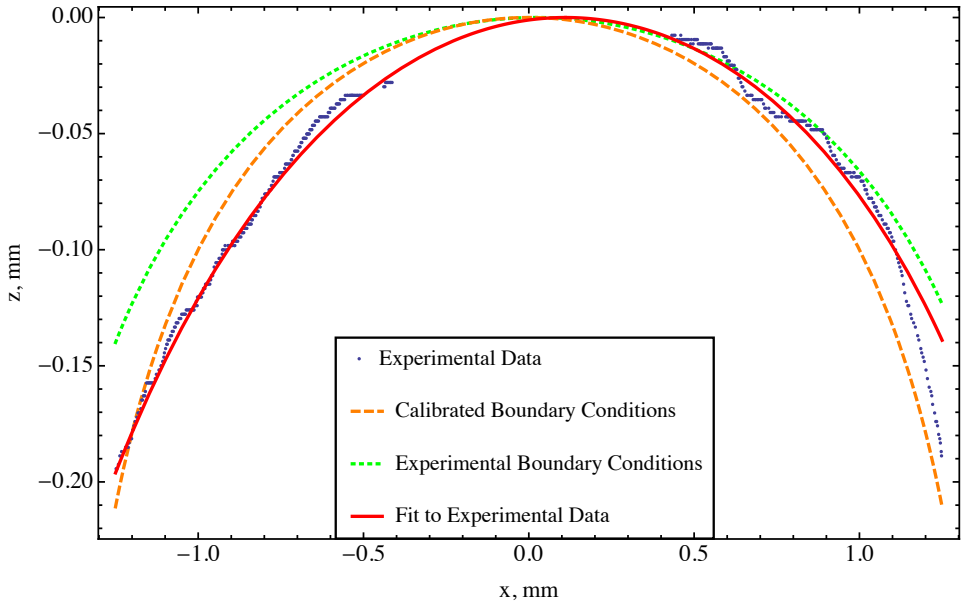

Fig. 4. Front curvature data and fits for the case of the 2.5 mm PBX 9501 layer.

the edge angles at each side of the PBX 9501 slab, which are used to generate front shapes with DSD. Angles on the right edge correspond to the unconfined PBX 9501 surface, while angles on the left correspond to the PBX 9502 interface.

Table 2. Error associated with front curvature fitting (expressed as the norm of the fit residuals) and edge angles computed from detonation-front fitting.

PBX 9501 Thickness (mm)	Fit Error (mm)	Edge Angle, Left (○)	Edge Angle, Right (○)
1.55	0.14	44.32	25.58
2.00	0.12	56.79	24.22
2.5	0.078	19.87	17.27

The results of Figs. 2-4 and Table 2 show that larger edge angles were observed on the PBX 9502 interface than on the side of the PBX 9501 slab exposed to the atmosphere. This is unexpected, given that PBX 9502 should provide at least as much confinement to the PBX 9501 as air. It is possible that imperfections in the bond between the two slabs led to high curvature near the slab interface. Also, it should be noted that the HMX crystals in PBX 9501 may be well in excess of 100 μm, which could possibly result in front-shape anomalies.

DSD Assuming Unconfined Boundary Conditions

DSD theory states that for a given explosive, there exists a relationship between the local curvature of the detonation front, κ, and the normal velocity, D_n. Given this relationship, it is possible to compute the steady-state shape of a detonation front in a rectangular slab of explosive. To apply DSD to the PBX 9501 slabs in our two-layer assemblies, the analysis can be simplified by assuming the PBX 9501 is unconfined on both sides. This assumption ignores the fact that one side of the PBX 9501 slab is bonded to PBX 9502, which provides a low, but possibly non-negligible level of confinement.

With this simplification, the application of DSD to the slab geometry is fairly routine. An established D_n-κ relationship for PBX 9501 is

$$\frac{D_n}{D_{CJ}} = 1 - B\kappa \left(\frac{1 + c_2 \left(B\kappa\right)^{e_2} + c_3 \left(B\kappa\right)^{e_3}}{1 + c_4 \left(B\kappa\right)^{e_4} + c_5 \left(B\kappa\right)^{e_5}} \right), \quad (1)$$

Table 3. PBX 9501 DSD parameters[6].

$D_{CJ_{nom}}$	8.811 mm/μs
$\rho_{0_{nom}}$	1.836 g/cm^3
κ_{max}	5 mm^{-1}
$B_{PBX9501}$	1.66374 mm
c_2	17.5036
c_3	3.15931
c_4	554.576
c_5	0.185264
c_6	0.861634
c_7	1.26499
ω_s	0.9408 rad

where $e_2 = e_4 = 1$ and $e_3 = e_5 = 2$, D_n is the local shock normal velocity, and κ the local shock curvature[6]. The DSD parameters are given in Table 3. The value of D_{CJ} used in Eq. 1 was computed for the experimentally measured densities using the equations

$$D_{CJ} = D_{CJ_{nom}}(1 + c_6(\rho_0/\rho_{0_{nom}} - 1)), \text{ and} \quad (2)$$

$$c_6 = \rho_0 \times 4.135/D_{CJ_{nom}}, \quad (3)$$

where ρ_0 is the measured density of the unreacted PBX 9501 slab. The value of B was also adjusted for density using the equation

$$B = B_{PBX9501}(\rho_0/\rho_{0_{nom}})^{c_7}. \quad (4)$$

The value of κ_{max} was increased to 5 mm^{-1} to extrapolate to the thinnest PBX 9501 sample. The parameter ω_s is the complement to the shock deflection angle, and the value was chosen assuming both faces of the PBX 9501 slab were exposed to atmospheric air. We can define the slope, $s = \mathrm{d}z/\mathrm{d}x$, and for a steady solution[7],

$$D_0 - D_n(\kappa)\ \left(1 + s^2\right)^{\frac{1}{2}} = 0 \quad (5)$$

where

$$\kappa = -\frac{\frac{\mathrm{d}s}{\mathrm{d}x}}{(1+s^2)^{\frac{3}{2}}} \quad (6)$$

for the slab geometry. Substituting Eqs. (1) and (6) into (5) results in an ODE that can be solved for $s(x)$, given an assumed value for D_0 and appropriate boundary conditions. The slope $s(x)$ can then be integrated, resulting in the DSD predicted front shape, $z(x)$.

The boundary conditions chosen for this analysis are to require the slope at the right edge of the slab to satisfy

$$s(z = z_{r\ edge}) = -\tan(\pi/2 - \omega_s), \quad (7)$$

and at the left edge,

$$s(z = z_{r\ edge}) = \tan(\pi/2 - \omega_s). \quad (8)$$

Iteration is then used to find the value of D_0 that satisfies these boundary conditions at both edges of the PBX 9501 slabs in each experiment. Results of this analysis are displayed as the dashed curve in Figs. 2–4.

DSD Assuming Experimental Edge Angles

One method to allow the DSD-generated front shapes to reflect the asymmetry caused by the PBX 9502 slab adjacent to the PBX 9501 is to use the edge angles determined by fitting, as listed in Table 2. The boundary conditions used to solve Eq. (5) are then

$$s(z = z_{r\ edge}) = -\tan(\phi_{right}) \quad (9)$$

at the right edge, and at the left edge

$$s(z = z_{r\ edge}) = \tan(\phi_{left}). \quad (10)$$

In these equations, ϕ_{right} is the unconfined (right) edge angle from Table 2, and ϕ_{left} is the edge angle on the PBX 9502 side. With these new boundary conditions, Eq. (5) can be solved as described in the previous section. The resulting front shapes are plotted in Figs. 2–4 using dotted lines.

Summary of Front-Shape DSD Predictions

The aforementioned DSD analysis can be used to predict PBX 9501 detonation front shapes and phase velocities in two-layer PBX 9501/9502 assemblies. For each of the experimental tests conducted, the phase velocities predicted by DSD using

both calibrated, unconfined edge angles and experimentally determined edge angles are listed in Table 4. In Figs. 2 and 3, it can be seen that the use of DSD with experimental boundary conditions results in better agreement with experiments than the use of boundary conditions calibrated for unconfined PBX 9501. In Fig. 4, DSD with calibrated boundary conditions appears to produce better agreement with the experimental front shape on the left (PBX 9502 interface) side, while producing worse agreement on the right (unconfined side). It is possible that for this experiment, the lack of data at the center resulted in less accurate edge angle results.

The results of Table 4 demonstrate that the phase velocity computed using DSD is fairly insensitive to the edge angle used to determine boundary conditions. The largest discrepancy between the two DSD computations is 18 m/s, for the case of the 2.5 mm PBX 9501. Except for this case, experimentally measured phase velocities are 20-30 m/s higher than DSD predictions. The use of the experimental edge angle improves the agreement with experiment slightly for the 1.55 mm and 2.00 mm cases, and substantially for the 2.5 mm case.

Table 4. Phase velocities measured experimentally, computed using calibrated, unconfined DSD edge angles, and computed using experimentally measured edge angles.

PBX 9501 Thickness (mm)	D_0, Experiment mm/μs	D_0, DSD - Calibrated Edge Angles mm/μs	D_0, DSD - Exp. Edge Angles mm/μs
1.55	8.638	8.612	8.616
2.00	8.696	8.672	8.674
2.5	8.731	8.716	8.734

Application of Shock Polar Analysis

Shock polar analysis may be applied to the simplified model of the PBX 9501/9502 interaction represented graphically in Fig. 5. In this model, the curved detonation front in the PBX 9501 slab is replaced with an oblique-planar detonation, with a shock angle chosen to represent either DSD front shapes or experimental data. Behind the PBX 9501 detonation, pressure in the detonation products is assumed to decrease isentropically in a release fan (these products are assumed to behave as a constant-γ ideal-gas). As seen in the figure, a PBX 9502 initiating layer shock is assumed to extend from the intersection of the PBX 9501 detonation with the interface between the two explosives. This shock structure divides the modeled explosive into five regions:

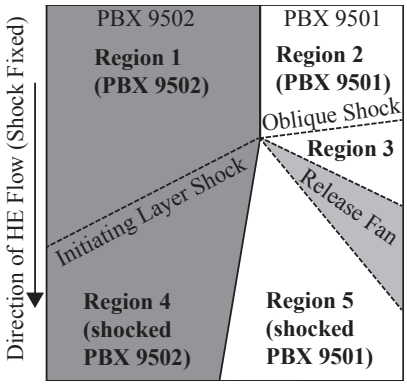

Fig. 5. Regions under consideration, and shock or detonation structures separating them (indicated by dashed lines). Dark gray indicates PBX 9502 while white coloring indicates PBX 9501. Light gray shading indicates the release fan. Regions 1 and 2 are under pressure equilibrium and Regions 4 and 5 are also under pressure equilibrium (at a different pressure); Region 3 only exists in the PBX 9501.

- Region 1: Unreacted PBX 9502 ahead of the PBX 9502 shock.
- Region 2: Unreacted PBX 9501 ahead of the PBX 9501 detonation. Regions 1 and 2 are in pressure equilibrium.
- Region 3: High pressure PBX 9501 product between the PBX 9501 detonation and release fan.
- Region 4: Shocked PBX 9502 (in pressure equilibrium with Region 5).
- Region 5: PBX 9501 detonation product (in pressure equilibrium with Region 4).

Pressure differentials between Regions 1 and 4 and Regions 2, 3, and 5 are maintained by shock structures which may be analyzed separately: the oblique detonation in the PBX 9501, the oblique-inert shock in the PBX 9502, and the release isentrope in the PBX 9501. An overview of the analysis strategy is presented below, followed by a detailed description of the analysis of each of these features.

Overview

To use this technique in a predictive fashion, a PBX 9501 shock angle would be chosen based on DSD front shape calculations. The phase velocity would also be determined by DSD. Then, a pseudo-Chapman-Jouguet (CJ) analysis would be used to compute the conditions in Region 3. A release isentrope could then be calculated which reduces the pressure from Region 3 to Region 5. For the DSD-determined phase velocity, a shock polar can be computed for the PBX 9502 oblique shock as well. Because pressure and streamline angle (θ) must be constant across Regions 4 and 5, the PBX 9501 release isentrope and PBX 9502 shock polar are presented in P-θ space in Fig. 6. The solution that satisfies this requirement occurs at the intersection of the PBX 9501 release isentrope (dashed curve) with the PBX 9502 shock polar (solid curve). The pressure at this solution is marked with a horizontal line for emphasis. This pressure could be combined with a Pop-plot to predict the initiating layer thickness. The analysis for the oblique shocks and release isentrope are described in detail below.

PBX 9502 Initiating-Layer Shock-Analysis

The initiating-layer shock in the PBX 9502 was assumed to be a planar oblique-shock. The oblique shock analysis was conducted by first considering a planar, normal shock, whose behavior is described by the Euler equations:

$$\rho_i \left(-D\right) = \rho \left(U_p - D\right), \tag{11}$$

$$p_i + \rho_i D^2 = p + \rho \left(U_p - D\right)^2, \text{and} \tag{12}$$

$$\frac{p_i}{\rho_i} + e_i + \frac{1}{2}D^2 = \frac{p}{\rho} + e + \frac{1}{2}\left(U_p - D\right)^2, \tag{13}$$

where ρ and ρ_i are the downstream and upstream densities, U_p is the downstream particle velocity in the laboratory frame, D is the shock velocity, p and p_i are the downstream and upstream pressures, and e and e_i are the downstream and upstream specific internal energies. Equations (11)-(13) can be simplified by assuming p_i is small relative to other terms.

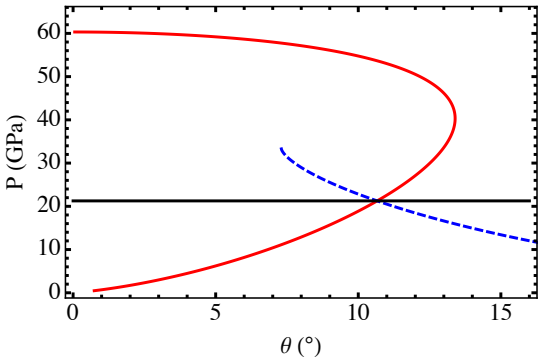

Fig. 6. Diagram showing PBX 9502 shock polar (solid curve), Region 4 and 5 pressure (horizontal line), and PBX 9501 release isentrope (dashed).

Equations (11)-(13), when combined with an EOS, can be solved to determine post-shock pressure given a value for shock velocity, D. For this analysis, the Mie-Grüneisen Keane EOS was used, and is described in detail by Aslam et. al[8]. The Mie-Grüneisen Keane parameters used for results reported here are $\rho_0 = 1.890$ g/cm^3, $K_0 = 6.5$ GPa, $K_0' = 23$, $K_\infty' = 4$, $\Gamma_0 = 0.5$, and $q = 1$.

The normal shock analysis can be extended to oblique planar shocks by replacing the shock velocity, D, with the oblique-shock normal velocity, D_n. D_n is related to the shock deflection angle, ϕ, and phase velocity, D_0, by the equation $D_n = D_0 \cos\phi$. To generate a shock polar such as the one in Fig. 6, we simply vary the shock angle ϕ from 0° to 90°, and plot the resulting pressures and corresponding streamline angles.

Table 5 lists experimentally measured initiating layer shock angles (ϕ) for each assembly tested. The streamline angles and Region 5 pressures were computed with Eqs. (11)-(13) and the PBX 9502 EOS. The pressures are also reported in column five of Table 6 for comparison to the model results.

Table 5. Experimentally measured initiating-layer shock-angle (ϕ) and corresponding streamline angle (θ) and pressure computed by applying shock-polar analysis to the PBX 9502 slabs.

PBX 9501 Thickness (mm)	Init. Layer ϕ (◦)	Region 4 Streamline Angle (◦)	Region 4 Pressure (GPa)
1.55	46.37	10.7	20.9
2.00	42.83	11.8	25.6
2.5	43.67	11.7	24.9

PBX 9501 Oblique Detonation Analysis

To analyze the PBX 9501 detonation, we make the assumption here that the curved detonation can be modeled as a planar-oblique detonation. This assumption greatly simplifies the analysis, but the trade-off is that the curvature of the detonation and its effects on the flow are neglected, and accuracy can suffer as a result. A more accurate treatment would be to use a reactive flow model, but the purpose of the present work is to determine the value of a simple, analytic model.

With this assumption, analysis of the PBX 9501 (white region of Fig. 5) was a two step process. The first step was to analyze the oblique detonation following the analysis of a CJ detonation described in Fickett and Davis[9]. Adjustment is made for the angle of the shock by equating D_{CJ} to the shock normal velocity: $D_{CJ} = D_n = D_0 \cos\phi$, where D_0 and ϕ are the phase velocity and shock angle from DSD analysis. With this value of D_{CJ}, the mass-specific heat release from detonation, q_{CJ}, can then be calculated with the equation from Fickett and Davis:

$$D_{CJ}^2 = 2(\gamma^2 - 1)q_{CJ}. \tag{14}$$

A γ value of 2.85 was assumed for this analysis. With q_{CJ} calculated from Eq. (14), pressure at the start of the release isentrope can be calculated using the equation

$$p = 2(\gamma - 1)\rho_0 q_{CJ}, \tag{15}$$

where ρ_0 is the density of the PBX 9501 upstream of the oblique shock. Similarly,

$$\rho = \rho_0(\gamma + 1)/\gamma, \tag{16}$$

$$c = D_{CJ}\gamma/(\gamma + 1), \text{ and} \tag{17}$$

$$e = \frac{p/\rho}{\gamma - 1} - q, \tag{18}$$

where c is the sound speed.

Analysis of PBX 9501 Release Isentrope

The release isentrope follows the PBX 9501 detonation and reduces the pressure in Region 3 to that of Region 5. With θ, p, ρ, c, and e specified at the head of the release isentrope, the conditions at any downstream density, ρ_d, within the isentrope can be calculated using the equations

$$p_d = \rho_d^{\gamma}\, p/\rho^{\gamma}, \tag{19}$$

$$e_d = \frac{p_d/\rho_d}{\gamma - 1} - q_{CJ}, \text{ and} \tag{20}$$

$$c_d = c\,(p_d/p)^{\frac{\gamma-1}{2\gamma}}, \tag{21}$$

where the subscript d indicates a downstream value. We also track the radial velocity within the isentrope, U_r, polar angle relative to a polar-coordinate system fixed at the head of the expansion fan, φ, and streamline angle, θ, using the equations developed by Bdzil and Stewart[10]:

$$U_{rd} = \sqrt{c^2 - c_d^2 + 2\,e - 2\,e_d + \frac{2\,p}{\rho} - \frac{2\,p_d}{\rho_d}}, \tag{22}$$

$$\varphi_d = \frac{U_{rd}}{c}, \text{ and} \tag{23}$$

$$\theta_d = \arctan\left(\frac{c_d\,\sin\varphi - U_{rd}\,\cos\varphi}{c_d\,\cos\varphi + U_{rd}\,\sin\varphi}\right). \tag{24}$$

Using the aforementioned PBX 9501 oblique detonation analysis and Eqs. (19)–(24) to describe the release isentrope, a release isentrope can be plotted in pressure vs. streamline angle space, as shown in Fig. 6.

Results and Discussion

Table 6 summarizes the results of experimental tests and model predictions for three PBX 9501/9502 assemblies with varying PBX 9501 layer thickness. In the second column, the PBX 9501 oblique shock angles required to generate the PBX 9502 initiating layer pressure associated with the observed initiating layer shock angles are listed for each experimental test (experimental phase velocities from Table 4 and the Mie-Grüneisen Keane EOS and PBX 9502 parameters described previously were also used to calculate PBX 9502 pressures). These pressures are listed in the fifth column.

Columns three and four list the PBX 9501 oblique shock angles computed by averaging the DSD front-shapes over the half of the slab closest to the PBX 9502 interface. Column three angles were generated assuming experimentally observed edge angles at the PBX 9502 interface, while column four angles were generated assuming the PBX 9501 edge angle calibrated from unconfined tests.

The pressures listed in columns six and seven of Table 6 are those predicted by the model for the PBX 9501 oblique shock angles of columns three and four. For the case of the 1.55 mm thick PBX 9501, the model prediction using asymmetric DSD boundary conditions is about 2.7 GPa low, while the prediction using symmetric DSD boundary conditions is lower by another 0.7 GPa.

The pressures predicted for the cases of the 2.00 and 2.5 mm thick PBX 9501 are significantly lower than the experimental values for both the asymmetric DSD boundary conditions and symmetric boundary conditions.

The pressures predicted with the present model are highly dependent on the angle assumed for the PBX 9501 detonation. Increasing the angle of the oblique detonation shifts the head of the release isentrope to lower pressure and higher streamline turning angle. As the PBX 9501 detonation angle is increased, the match point between the PBX 9502 polar and PBX 9501 release isentrope increases and then decreases in pressure. For example, for the case of the 1.55 mm PBX 9501, the highest match pressure predicted by the model is 19.6 GPa at a PBX 9501 detonation angle of 25°. Similarly, for the other two cases, the highest match pressure is between 19.5 and 20 GPa and an angle of approximately 25°.

Summary and Conclusions

A method combining DSD front shape and phase velocity calculations with polar matching was used to analyze the interaction between adjacent, detonating PBX 9501 and PBX 9502 slabs. In the analysis, the shock angles from DSD are used with the DSD-predicted phase velocity to compute the shock polars for each slab and determine the pressure associated with the PBX 9502 initiating layer shock. This method makes a number of assumptions, and one of the sources of error arises from the extraction of an oblique shock angle from the curved PBX 9501 DSD front shape for use in polar analysis. The technique chosen here was to average the shock angle over the half of the PBX 9501 slab closest to the

Table 6. Results of initiating layer pressure predictions, and the PBX 9502 oblique shock angles used to obtain them.

PBX 9501 Thickness (mm)	Shock Angle, Expt. (○)	Avg. Shock Angle, Asym. DSD, Left (○)	Avg. Shock Angle, Sym. DSD, Left (○)	Init. Layer Pres., Expt. (GPa)	Init. Layer Pres., Asym. DSD (GPa)	Init. Layer Pres., Sym. DSD (GPa)
1.55	9.13	14.5	12.0	20.9	18.2	17.5
2.00	13.8	15.2	10.7	25.6	18.5	17.3
2.5	12.9	6.39	9.57	24.9	16.2	17.1

PBX 9502 interface, rather than use the PBX 9501 shock edge angle at the PBX 9502 interface. This resulted in initiating layer shock pressures lower than those indicated by experimentally measured initiating layer shock angles. The best agreement appears to be obtained using PBX 9501 shock angles near 25°, suggesting that initiating layer behavior is dependent on the detonation behavior of a significant portion of the PBX 9501 slab rather than just the portion closest to the PBX 9502 interface. It is likely that incorporating full reactive flow simulations can yield suitable results, but at much higher computational expense.

Acknowledgements

This effort was funded by the U.S. Department of Energy Campaign 2: "Dynamic Material Properties."

References

1. E. K. Anderson, T. D. Aslam, and S. I. Jackson, "Transverse initiation of an insensitive explosive in a layered slab geometry: Front shapes and post-shock flow measurements," *Combustion and Flame* , 2014. http://dx.doi.org/10.1016/j.combustflame.2013.12.023, In Press.

2. E. K. Anderson, T. D. Aslam, and S. I. Jackson, "Transverse initiation of an insensitive explosive in a layered slab geometry," *AIP Conference Proceedings* , 2013. Shock Compression of Condensed Matter, In Press.

3. E. Anderson, T. Aslam, and S. Jackson, "The effect of transverse shock propagation on the shock-to-detonation transition process for an insensitive explosive," in *Proceedings of the Combustion Institute*, **Submitted**, p. In press., Elsevier, 2014.

4. C. Matignon, R. Sorin, and O. Bozier, "Detonation propagation of converging front in ihe: Comparison of direct numerical simulation and detonation shock dynamics agains experimental data," in *Fourteenth Symposium (Int.) on Detonation*, pp. 1182–1190, Office of Naval Research, 2010.

5. S. I. Jackson and M. Short, "Determination of the velocity-curvature relationship for unknown front shapes," *AIP Conference Proceedings* **1426**(1), pp. 347–350, 2012.

6. T. Aslam and M. Short, "Detonation shock dynamics overview and calibration," Tech. Rep. LA-UR-13-26358, Los Alamos National Laboratory, 2013.

7. T. Aslam, "Detonation shock dynamics calibration of PBX 9501," *AIP Conference Proceedings* **955**(1), p. 813, 2007.

8. T. D. Aslam, R. Gustavsen, N. Sanchez, and B. D. Bartram, "An equation of state for polymethylpentene (TPX) including multi-shock response," *AIP Conference Proceedings* **1426**(1), pp. 767–770, 2012.

9. W. Fickett and W. Davis, *Detonation Theory and Experiment*, Dover, New York, 2000.

10. J. Bdzil and D. Stewart, "Theory of detonation shock dynamics," *Shock Wave Science and Technology Reference Library* **6**, pp. 373–453, 2012.